BRUSSELS–MONTREAL NUCLEAR ENERGY DENSITY FUNCTIONALS, FROM ATOMIC MASSES TO NEUTRON STARS*

N. Chamel[a], J.M. Pearson[b], A.F. Fantina[a], C. Ducoin[c]
S. Goriely[a], A. Pastore[a]

[a]Institut d'Astronomie et d'Astrophysique, Université Libre de Bruxelles
1050 Brussels, Belgium
[b]Département de Physique, Université de Montréal
Montréal (Québec), H3C 3J7, Canada
[c]Institut de Physique Nucléaire de Lyon, Domaine scientifique de la Doua
Bât. Paul Dirac, 4 Rue Enrico Fermi, 69622 Villeurbanne Cedex, France

(Received January 21, 2015)

We have recently developed a series of accurately calibrated nuclear energy density functionals, fitted to essentially all atomic masses with a model root mean square deviation now reduced to 0.5 MeV for our functional BSk27*. At the same time, these functionals were adjusted to realistic equations of state of neutron matter and were constrained to reproduce various properties of nuclear matter. Using BSk27*, we have calculated the internal constitution and the equation of state of the crust of non-accreting neutron stars.

DOI:10.5506/APhysPolB.46.349
PACS numbers: 21.10.Dr, 21.60.Jz, 26.60.Gj, 26.60.Kp

1. Introduction

The nuclear energy density functional (EDF) theory aims at providing a universal description of various nuclear systems, from atomic nuclei [1] to extreme astrophysical environments like neutron stars and supernova cores [2]. A recent overview of the complete formalism can be found in Ref. [3]. The main limitation of the EDF theory stems from the functional itself, whose exact form is unknown. For this reason, various phenomenological functionals have been proposed. These functionals have been traditionally obtained from density-dependent effective nucleon–nucleon interactions in the

* Presented at the Zakopane Conference on Nuclear Physics "Extremes of the Nuclear Landscape", Zakopane, Poland, August 31–September 7, 2014.

framework of the self-consistent mean-field methods, namely the Hartree–Fock (HF) or Hartree–Fock–Bogoliubov (HFB) approximations depending on whether nuclear pairing is taken into account or not. The ensuing EDFs are generally non-local, but can reduce to a semi-local form for zero-range effective interactions of the Skyrme type [1, 2]. These interactions have been widely employed since they allow for very fast numerical computations. Although such a formulation based on effective interactions imposes stringent restrictions on the form of the EDF, it guarantees the cancellation of the internal energy in the limiting case of one nucleon [4]. On the other hand, the EDFs may still be contaminated by many-body self-interactions errors (see, *e.g.*, Ref. [3]).

Once a specific form of the effective interaction is postulated, the associated parameters need to be adjusted to reproduce a selected set of nuclear data. The non-uniqueness of the fitting procedure has led to a large number of different parametrizations. Some of them may yield very different predictions when applied outside the domain where they were fitted [5]. This situation is particularly unsatisfactory for nuclear astrophysical applications which require a knowledge of nuclear masses for nuclei so neutron rich that there is no hope of measuring them in the foreseeable future; such nuclei are found in the outer crust of neutron stars [6–8]. Extrapolations far beyond the neutron drip line are required for the description of the inner crust of neutron stars where neutron–proton clusters coexist with unbound neutrons (see, *e.g.*, Ref. [9]). On the other hand, the reliability of phenomenological EDFs for very neutron-rich systems can be tested by comparing their predictions for the properties of pure neutron matter with the results obtained from microscopic calculations based on realistic nucleon–nucleon potentials. The properties of high-density matter can be also studied via heavy-ion collision experiments. For this reason, we have developed a series of accurately calibrated semi-local EDFs fitted to essentially all measured atomic mass data, while imposing additional constraints on the EDF. After briefly reviewing our recent progress, applications to the description of the crust of non-accreting neutron stars will be presented using the latest of our series, the BSk27* EDF.

2. Brussels–Montreal nuclear energy density functionals

The Brussels–Montreal (BSk) series of EDFs were obtained from zero-range effective interactions. As in conventional superconductors, the effective interaction governing single-particle properties may not necessarily be the same as the interaction responsible for nuclear pairing. For the former, we considered generalized Skyrme effective interactions of the form

$$
\begin{aligned}
v(\boldsymbol{r}_i,\boldsymbol{r}_j) \;=\; & t_0(1+x_0P_\sigma)\delta(\boldsymbol{r}_{ij}) + \frac{1}{2}t_1(1+x_1P_\sigma)\frac{1}{\hbar^2}\left[p_{ij}^2\,\delta(\boldsymbol{r}_{ij}) + \delta(\boldsymbol{r}_{ij})\,p_{ij}^2\right] \\
& + t_2(1+x_2P_\sigma)\frac{1}{\hbar^2}\boldsymbol{p}_{ij}\cdot\delta(\boldsymbol{r}_{ij})\,\boldsymbol{p}_{ij} + \frac{1}{6}t_3(1+x_3P_\sigma)n(\boldsymbol{r})^\alpha\,\delta(\boldsymbol{r}_{ij}) \\
& + \frac{1}{2}\,t_4(1+x_4P_\sigma)\frac{1}{\hbar^2}\left[p_{ij}^2\,n(\boldsymbol{r})^\beta\,\delta(\boldsymbol{r}_{ij}) + \delta(\boldsymbol{r}_{ij})\,n(\boldsymbol{r})^\beta\,p_{ij}^2\right] \\
& + t_5(1+x_5P_\sigma)\frac{1}{\hbar^2}\boldsymbol{p}_{ij}n(\boldsymbol{r})^\gamma\,\delta(\boldsymbol{r}_{ij})\,\boldsymbol{p}_{ij} \\
& + \frac{\mathrm{i}}{\hbar^2}W_0\,(\hat{\boldsymbol{\sigma}}_{\boldsymbol{i}}+\hat{\boldsymbol{\sigma}}_{\boldsymbol{j}})\,\boldsymbol{p}_{ij}\times\delta(\boldsymbol{r}_{ij})\,\boldsymbol{p}_{ij}\,, \qquad (1)
\end{aligned}
$$

where $\boldsymbol{r}_{ij} = \boldsymbol{r}_i - \boldsymbol{r}_j$, $\boldsymbol{r} = (\boldsymbol{r}_i + \boldsymbol{r}_j)/2$, $\boldsymbol{p}_{ij} = -\mathrm{i}\hbar(\boldsymbol{\nabla}_i - \boldsymbol{\nabla}_j)/2$ is the relative momentum, $\hat{\boldsymbol{\sigma}}_{\boldsymbol{i}}$ and $\hat{\boldsymbol{\sigma}}_{\boldsymbol{j}}$ are Pauli spin matrices, P_σ is the two-body spin-exchange operator, and $n(\boldsymbol{r})$ denotes the average nucleon number density. As for the pairing interaction, we considered effective interactions of the form

$$
v(\boldsymbol{r}_i,\boldsymbol{r}_j) = v^\pi(n_n(\boldsymbol{r}), n_p(\boldsymbol{r}))\delta(\boldsymbol{r}_{ij})\,, \qquad (2)
$$

where $n_n(\boldsymbol{r})$ and $n_p(\boldsymbol{r})$ denote the average neutron and proton number densities respectively. In order to regularize the ultra-violet divergences arising from the zero range of the interaction, some cutoff has to be imposed, either in the quasiparticle or in the single-particle energy spectrum. Because of Coulomb effects, the proton pairing strength is expected to be different from the neutron pairing strength. Since we use the equal-filling approximation [10], we must also allow the pairing strength to be slightly stronger for nucleons of which there are an odd number. Indeed, this procedure can be understood microscopically [11] as compensating for the neglect of the time-odd fields. (Note that the odd nucleon will nevertheless contribute to the time-even fields.) We take account of these extra degrees of freedom by multiplying the pairing strength, as determined through Eq. (2), by renormalising factors f_n^-, f_p^+ and f_p^- (we set $f_n^+ \equiv 1$).

The parameters of these effective interactions were determined primarily by fitting all measured atomic masses from the Atomic Mass Evaluations (AME) [12, 13] with $Z, N \geq 8$. At the same time, an optimal fit to charge radii was ensured. In an attempt to account for dynamical correlations, we have subtracted from the HFB energy an estimate for the spurious collective energy. As described in Ref. [14], the form we adopted in our HFB-16 model and all subsequent models is

$$
E_{\mathrm{coll}} = E_{\mathrm{rot}}^{\mathrm{crank}}\left\{b\ \tanh(c|\beta_2|) + d|\beta_2|\ \exp\left\{-l\left(|\beta_2| - \beta_2^0\right)^2\right\}\right\}\,, \qquad (3)
$$

in which $E_{\mathrm{rot}}^{\mathrm{crank}}$ denotes the cranking-model value of the rotational correction and β_2 the quadrupole deformation. To the HFB energy, we also add a

phenomenological Wigner correction,

$$E_{\rm W} = V_{\rm W} \exp\left\{-\lambda\left(\frac{N-Z}{A}\right)^2\right\} + V'_{\rm W}|N-Z| \exp\left\{-\left(\frac{A}{A_0}\right)^2\right\}, \quad (4)$$

which contributes significantly only for light nuclei ($A < A_0$) or nuclei with N close to Z (see, *e.g.*, Ref. [14] for a discussion of the physical interpretation of these terms). The spurious centre-of-mass energy is removed following an essentially exact procedure [15]. Moreover, a correction for the finite size of the proton is made to both the charge radius and the energy [14]. Finally, we drop Coulomb exchange, thus simulating neglected effects such as Coulomb correlations, charge-symmetry breaking, and vacuum polarization [16]. A detailed description of the fitting procedure can be found in Ref. [17].

Our ultimate aim is to construct a universal nuclear EDF that could be reliably applied to study not only the properties of atomic nuclei but also the interior of neutron stars and supernova cores. To this end, we have been imposing on our mass models an increasing number of relevant constraints. The progress made so far over the past years can be summarized as follows (see Ref. [14] for a review of our older models):

— BSk16 [14] was fitted to the $^1S_0$ pairing gaps in pure neutron matter, as obtained from BCS calculations using realistic nucleon–nucleon potentials; BSk17 [18] was fitted to diagrammatic calculations of the $^1S_0$ pairing gaps including medium polarization effects, both in pure neutron matter and in symmetric nuclear matter (see also Ref. [19]). In this way, we showed that the pairing strength can be uniquely determined from the $^1S_0$ pairing gap function $\Delta_q(n_n, n_p)$ in asymmetric homogeneous nuclear matter, and can be accurately expressed as ($q = n, p$ for neutrons and protons respectively) [20]

$$v_q^\pi(n_n, n_p) = -\frac{8\pi^2}{\sqrt{\varepsilon_{\rm F}^{(q)}}}\left(\frac{\hbar^2}{2M_q^*}\right)^{3/2}\left[2\ln\left(\frac{2\varepsilon_{\rm F}^{(q)}}{\Delta_q}\right) + \Lambda\left(\frac{\varepsilon_\Lambda}{\varepsilon_{\rm F}^{(q)}}\right)\right]^{-1}, \quad (5)$$

$$\Lambda(x) = \ln(16x) + 2\sqrt{1+x} - 2\ln\left(1+\sqrt{1+x}\right) - 4, \quad (6)$$

$\varepsilon_{\rm F}^{(q)} = \hbar^2(3\pi^2 n_q)^{2/3}/(2M_q^*)$ (M_q^* is the nucleon effective mass) and ε_Λ is a single-particle energy cutoff above the Fermi level. An optimum fit to atomic masses was achieved for $\varepsilon_\Lambda = 16$ MeV.

— t_4 and t_5 terms were introduced in BSk18 [21] to prevent the ferromagnetic collapse of neutron stars.

— Making use of the flexibility allowed by the t_4 and t_5 terms, BSk19, BSk20, and BSk21 [22] were fitted to three different realistic neutron-matter equations of state (EoS) with different degrees of stiffness, reflecting the current lack of knowledge of the high-density behaviour of dense matter. In addition, the terms quadratic in the spin-current tensor and their time-odd counterpart from the EDF were dropped. This prescription not only avoids the occurrence of spurious long wavelength spin and spin–isospin instabilities, but also substantially improves the values of the Landau parameters [23]. Although finite-size instabilities may still arise, the instability window is dramatically reduced [24].

— Whereas all previous models described above were fitted to a symmetry energy coefficient $J = 30$ MeV, other values ranging from 29 to 32 MeV were considered in the series from BSk22 to BSk26 [17]. The best fit to atomic masses was achieved for $J = 29$–30 MeV. Such values are also supported by measurements of neutron-skin thicknesses of various neutron-rich nuclei [17]. The values for the slope of the symmetry energy obtained with these EDFs lie in the range of $L = 37.5$–68.5 MeV, in close agreement with various empirical constraints [25, 26].

— BSk27* [27] is based on standard Skyrme and pairing interactions that could be more easily implemented in existing HF(B) codes. It yields the optimal fit of the 2353 measured masses of nuclei with N and $Z \geq 8$ appearing in the 2012 AME [13], with a model standard deviation as low as $\sigma_{\rm mod} = 0.500$ MeV.

In all cases, the incompressibility K_v of symmetric nuclear matter at saturation was required to fall in the empirical range 240 ± 10 MeV [28]. Moreover, the isoscalar effective mass in symmetric nuclear matter at saturation was fixed to the realistic value $M^*_{\rm s} = 0.8$ (see Ref. [29] for a summary of the experimental and theoretical evidence). Although our EDFs were adjusted to realistic EoS of pure neutron matter only, the EoS of symmetric nuclear matter obtained from our EDFs are compatible with the constraints inferred from the analysis of heavy-ion collision experiments [30, 31]. Moreover, the isovector effective mass M^*_v is found to be smaller than $M^*_{\rm s}$ at the saturation density, implying thereby that $M^*_n > M^*_p$ in neutron-rich matter. This result is consistent with measurements of isovector giant resonances [32], and microscopic calculations [33, 34]. The predictions of our EDFs for high-density nuclear matter can be further tested using neutron-star observations [35].

3. Application to neutron stars

Born in the aftermath of gravitational core-collapse supernova explosions, neutron stars are the densest stars known in the universe and are even more compact than the heaviest atomic nuclei [36]. With average mass densities ranging from a few grams per cubic centimetres at their surface to about 10^{15} g cm^{-3} at their centre, neutron stars are expected to exhibit very different phases of matter, thus making them unique laboratories to study the properties of dense matter. According to our current understanding, a neutron star contains several distinct regions, which can be classified as follows with increasing depth [36].

— A very thin atmospheric plasma layer of light elements (mainly hydrogen and helium though heavier elements like carbon may also be present) possibly surrounds a Coulomb liquid of electrons and ions.

— Below these liquid surface layers, the matter consists of a crystal lattice of fully ionized atoms thus forming a solid crust. With increasing density, nuclei become progressively more neutron rich until neutrons start to drip out of nuclei as the average baryon number density reaches $\bar{n} \sim 2.5 \times 10^{-4}$ fm^{-3} (see Table I). The inner layers of the crust are thus permeated by a neutron ocean, which is superfluid at low temperatures $T < T_c$.

— The crust extends up to about half saturation density above which it dissolves into an homogeneous liquid mixture of nucleons and leptons (see Table II). The innermost part of the core may contain other particles such as hyperons or even deconfined quarks.

TABLE I

Proton number Z, mass number A, density $\bar{n}_{\rm drip}$, and pressure $P_{\rm drip}$ at the neutron-drip transition for two different atomic mass models.

	Z	A	$\bar{n}_{\rm drip}$ [fm^{-3}]	$P_{\rm drip}$ [MeV fm^{-3}]
HFB-21	38	124	2.57×10^{-4}	4.89×10^{-4}
HFB-27*	38	122	2.51×10^{-4}	4.84×10^{-4}

TABLE II

Density $\bar{n}_{\rm cc}$, electron fraction Y_e and pressure $P_{\rm cc}$ at the crust–core transition for two different nuclear energy density functionals.

	$\bar{n}_{\rm cc}$ [fm^{-3}]	Y_e	$P_{\rm cc}$ [MeV fm^{-3}]
BSk21	0.0809	0.0335	0.269
BSk27*	0.0919	0.0383	0.439

Observations from ground- and space-based instruments have led to the discovery of remarkable astrophysical phenomena that are thought to be intimately related to the physics of neutron-star crusts like pulsar sudden spin-ups (so-called "glitches"), the thermal relaxation of quasipersistent soft X-ray transients, X-ray bursts, and quasiperiodic oscillations in soft-gamma ray repeaters (see, *e.g.*, Ref. [9]). The crust composition is also essential to evaluate the possible contribution of neutron stars to the galactic enrichment in the so-called r-process nuclei [37]. During the supernova explosion and the subsequent evolution, it is reasonable to assume that all kinds of nuclear and electroweak processes are allowed so that the compressed matter in the stellar remnant eventually reaches its ground state as the newly born neutron star cools down. This so-called cold catalysed matter hypothesis implies that all neutron stars can be described by the same EoS. This assumption is certainly not valid in the crust of accreting neutron stars, but we shall not study this case here. As in the seminal paper from Baym, Pethick and Sutherland [38] the outer crust is supposed to be made of only one type of nuclide arranged in a body-centred cubic lattice and coexisting with a degenerate electron gas. The only microscopic inputs are nuclear masses, for which we have used the experimental data from the 2012 AME [13] complemented with our latest nuclear mass model HFB-27* [27] for the masses that have not yet been measured. The resulting composition, obtained using the same method as in Ref. [6], is shown in Table III. The sequence of equilibrium nuclides differs from that previously obtained with HFB-21 [6]. In particular, the presence of the odd nuclei ^{79}Cu and ^{121}Y predicted by HFB-21, is no longer supported by HFB-27*. Likewise HFB-27* predicts neither the presence of ^{80}Ni nor ^{124}Sr in the outer crust. On the other hand, HFB-27* does predict the appearance of ^{126}Ru and ^{124}Zr, contrary to HFB-21. The two atomic mass models also differ in their predictions of the neutron drip transition, as shown in Table I. The root-mean-square deviation to the 2012 AME data is $\sigma = 0.51$ MeV for HFB-27* [27], as compared to $\sigma = 0.57$ MeV for HFB-21 [17]; although HFB-21 was fitted to the 2003 AME data, it yields an even better fit to the 2012 AME. The discrepancies between these two models for the composition of neutron-star crust arise from the uncertainties in the masses of neutron-rich nuclei. For instance, the values for the mass of ^{124}Sr as calculated with HFB-21 and HFB-27* are found to differ by about 2.4 MeV. A study of the model and parameter uncertainties affecting the HFB mass predictions can be found in Ref. [5]. For the inner crust, we have employed the semiclassical Thomas–Fermi approach extended up to the fourth order using the BSk27* EDF underlying the HFB-27* nuclear mass model applied in the outer crust. Proton shell effects were included using the Strutinsky integral theorem (see Ref. [39] for details). Neutron shell effects are known to be much smaller and were therefore neglected [40].

TABLE III

Sequence of equilibrium nuclides with increasing depth in the outer crust of a non-accreting neutron star for the HFB-27* atomic mass model. The nuclides with experimentally measured masses are indicated in boldface. Indicated are also the minimum density $\bar{n}_{\rm min}$, the maximum density $\bar{n}_{\rm max}$ and the maximum pressure $P_{\rm max}$ at which each nuclide can be found.

	$\bar{n}_{\rm min}$ [fm^{-3}]	$\bar{n}_{\rm max}$ [fm^{-3}]	$P_{\rm max}$ [MeV fm^{-3}]
^{56}**Fe**	–	4.90×10^{-9}	3.33×10^{-10}
^{62}**Ni**	5.05×10^{-9}	1.63×10^{-7}	4.36×10^{-8}
^{64}**Ni**	1.69×10^{-7}	8.01×10^{-7}	3.56×10^{-7}
^{66}**Ni**	8.26×10^{-7}	8.66×10^{-7}	3.79×10^{-7}
^{86}**Kr**	8.84×10^{-7}	1.88×10^{-6}	1.05×10^{-6}
^{84}**Se**	1.94×10^{-6}	6.87×10^{-6}	5.66×10^{-6}
^{82}**Ge**	7.11×10^{-6}	1.69×10^{-5}	1.79×10^{-5}
^{80}**Zn**	1.75×10^{-5}	3.53×10^{-5}	4.56×10^{-5}
^{78}Ni	3.68×10^{-5}	7.10×10^{-5}	1.10×10^{-4}
^{126}Ru	7.40×10^{-5}	7.64×10^{-5}	1.14×10^{-4}
^{124}Mo	7.86×10^{-5}	1.31×10^{-4}	2.27×10^{-4}
^{122}Zr	1.35×10^{-4}	1.63×10^{-4}	2.91×10^{-4}
^{124}Zr	1.66×10^{-4}	1.88×10^{-4}	3.43×10^{-4}
^{120}Sr	1.91×10^{-4}	1.95×10^{-4}	3.54×10^{-4}
^{122}Sr	1.99×10^{-4}	2.51×10^{-4}	4.84×10^{-4}

The procedure just described is a computationally very fast approximation to the full HF equations. The proton number $Z = 40$ is found to be favoured in all layers, in agreement with the results obtained with BSk21 [39]. On the other hand, BSk27* yields a stiffer EoS, as shown in Fig. 1; this behaviour

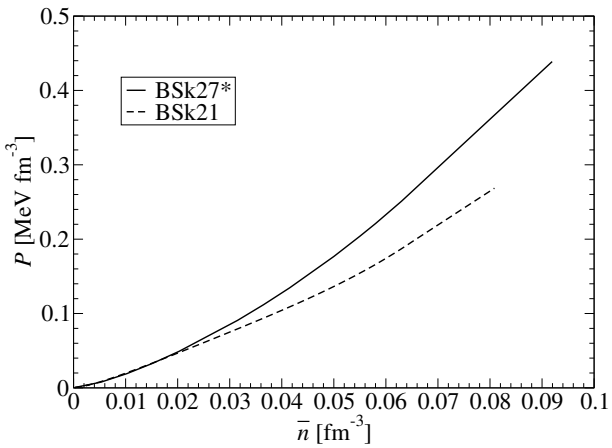

Fig. 1. Pressure *vs.* average baryon number density in the crust of a non-accreting neutron star, as predicted by two different nuclear energy density functionals.

arises from the correspondingly stiffer neutron-matter EoS at subsaturation densities [27]. The properties of the crust–core transition, as calculated by the method described in Ref. [41] (see also Ref. [39]), are indicated in Table II. The higher values for the crust–core transition density and pressure obtained with BSk27* can be traced back to the much lower value for the slope of the symmetry energy [42]: $L = 28.5$ MeV for BSk27*, as compared to $L = 46.6$ MeV for BSk21.

4. Conclusion

We have employed BSk27*, the latest of the accurately calibrated Brussels–Montreal EDFs, to determine the structure, the composition and the EoS of non-accreting neutron-star crusts. The results differ substantially from those previously obtained using BSk21. To a large extent, these discrepancies arise from the different degrees of stiffness of the underlying neutron-matter equations of state. The EDF theory can be also applied to study the properties of matter at still higher densities, but BSk27* is not suitable for this purpose as its EoS is found to be too soft to support the recently observed neutron stars with a mass close to two solar masses.

This work was supported by FNRS, Belgium, NSERC, Canada and the COST action MP1304.

REFERENCES

[1] M. Bender, P.-H. Heenen, P.-G. Reinhard, *Rev. Mod. Phys.* **75**, 121 (2003).
[2] J.R. Stone, P.-G. Reinhard, *Prog. Part. Nucl. Phys.* **58**, 587 (2007).
[3] T. Duguet, *Lec. Notes Phys.* **879**, 293 (2014).
[4] N. Chamel, *Phys. Rev.* **C82**, 061307(R) (2010).
[5] S. Goriely, R. Capote, *Phys. Rev.* **C89**, 054318 (2014).
[6] J.M. Pearson, S. Goriely, N. Chamel, *Phys. Rev.* **C83**, 065810 (2011).
[7] R.N. Wolf *et al.*, *Phys. Rev. Lett.* **110**, 041101 (2013).
[8] S. Kreim, M. Hempel, D. Lunney, J. Schaffner-Bielich, *Int. J. Mass Spec.* **349–350**, 63 (2013).
[9] N. Chamel, P. Haensel, *Living Rev. Relativ.* **11**, 10 (2008) `http://www.livingreviews.org/lrr-2008-10`
[10] S. Perez-Martin, L.M. Robledo, *Phys. Rev.* **C78**, 014304 (2008).
[11] G.F. Bertsch *et al.*, *Phys. Rev.* **C79**, 034306 (2009).
[12] G. Audi, A.H. Wapstra, C. Thibault, *Nucl. Phys.* **A729**, 337 (2003).
[13] G. Audi *et al.*, *Chin. Phys.* **C36**, 1287 (2012).

[14] N. Chamel, S. Goriely, J.M. Pearson, *Nucl. Phys.* **A812**, 72 (2008).
[15] S. Goriely, M. Samyn, M. Bender, J.M. Pearson, *Phys. Rev.* **C68**, 054325 (2003).
[16] S. Goriely, J.M. Pearson, *Phys. Rev.* **C77**, 031301 (2008).
[17] S. Goriely, N. Chamel, J.M. Pearson, *Phys. Rev.* **C88**, 024308 (2013).
[18] S. Goriely, N. Chamel, J.M. Pearson, *Phys. Rev. Lett.* **102**, 152503 (2009).
[19] S. Goriely, N. Chamel, J.M. Pearson, *Eur. Phys. J.* **A42**, 547 (2009).
[20] N. Chamel, *Phys. Rev.* **C82**, 014313 (2010).
[21] N. Chamel, S. Goriely, J.M. Pearson, *Phys. Rev.* **C80**, 065804 (2009).
[22] S. Goriely, N. Chamel, J.M. Pearson, *Phys. Rev.* **C82**, 035804 (2010).
[23] N. Chamel, S. Goriely, *Phys. Rev.* **C82**, 045804 (2010).
[24] A. Pastore *et al.*, *Phys. Rev.* **C90**, 025804 (2014).
[25] M.B. Tsang *et al.*, *Phys. Rev.* **C86**, 015803 (2012).
[26] C.J. Horowitz *et al.*, *J. Phys. G: Nucl. Part. Phys.* **41**, 093001 (2014).
[27] S. Goriely, N. Chamel, J.M. Pearson, *Phys. Rev.* **C88**, 061302(R) (2013).
[28] G. Colò *et al.*, *Phys. Rev.* **C70**, 024307 (2004).
[29] S. Goriely, M. Samyn, J.M. Pearson, *Phys. Rev.* **C75**, 064312 (2007).
[30] P. Danielewicz, R. Lacey, W.G. Lynch, *Science* **298**, 1592 (2002).
[31] W.G. Lynch *et al.*, *Prog. Part. Nucl. Phys.* **62**, 427 (2009).
[32] T. Lesinski, K. Bennaceur, T. Duguet, J. Meyer, *Phys. Rev.* **C74**, 044315 (2006).
[33] E.N.E. van Dalen, C. Fuchs, A. Faessler, *Phys. Rev. Lett.* **95**, 022302 (2005).
[34] W. Zuo, U. Lombardo, H.-J. Schulze, Z.H. Li, *Phys. Rev.* **C74**, 014317 (2006).
[35] A.F. Fantina, N. Chamel, J.M. Pearson, S. Goriely, *Astron. Astrophys.* **559**, A128 (2013).
[36] P. Haensel, A.Y. Potekhin, D.G. Yakovlev, *Neutron Stars 1: Equation of State and Structure*, Springer, 2007.
[37] S. Goriely, A. Bauswein, H.-T. Janka, *Astrophys. J.* **738**, L32 (2011).
[38] G. Baym, C. Pethick, P. Sutherland, *Astrophys. J.* **170**, 299 (1971).
[39] J.M. Pearson, N. Chamel, S. Goriely, C. Ducoin, *Phys. Rev.* **C85**, 065803 (2012).
[40] K. Oyamatsu, M. Yamada, *Nucl. Phys.* **A578**, 181 (1994).
[41] C. Ducoin, Ph. Chomaz, F. Gulminelli, *Nucl. Phys.* **A789**, 403 (2007).
[42] C. Ducoin, J. Margueron, C. Providência, I. Vidaña, *Phys. Rev.* **C83**, 045810 (2011).